Enhanced Defect Detection and Characterisation by Signal Processing of Ultrasonic Array Data

Paul D. WILCOX, Caroline HOLMES, Bruce W. DRINKWATER, Department of Mechanical Engineering, University of Bristol, University Walk, Bristol, UK.

Abstract. The full data set from an ultrasonic array comprises the time-domain signals from every possible transmitter-receiver pair in the array. The possibility of experimentally obtaining the full data set that is afforded by some new array controller systems massively increases the potential of ultrasonic arrays. Firstly, any conventional array imaging procedure (e.g. B-scans, angular scans, dynamic depth focusing) can be performed by post-processing the information in the full data set. More importantly, the full data set enables imaging techniques to be developed that have no direct counterpart in conventional ultrasonics. For example, the authors have previously shown that the total focusing method (TFM) outperforms other standard linear processing techniques when imaging a point reflector. This is because the TFM represents the complete array being focused in transmission and reception at every point in an image. In this paper two advanced versions of the TFM are described. The first called the vector TFM (VTFM) algorithm allows the angular reflectivity characteristics of any point in a sample to be obtained. This has obvious advantages for defect sizing and classification. The VTFM algorithm probes the scattering behaviour of a defect over a range of angles. The response is displayed as a vector that represents defect orientation and a scalar quantity that represents the specularity of the reflector. Both simulated and experimental results are shown from which the orientation of small reflectors is determined and visualised. The second algorithm is termed the diffraction TFM (DTFM) and uses a pair of arrays in a similar manner to time-of-flight diffraction (TOFD) systems. The immediate advantage of DTFM over TOFD is the ability to produce a B-scan image without moving the transducers. Potential additional advantages are superior sensitivity and the ability to overlay pulse-echo information from back-scattered signals with pitch-catch information from diffracted signals. Experimental results are presented from an industrial weld sample containing a number of realistic defects.

1. Introduction

Ultrasonic arrays for NDE are now routinely used in industry due to the flexibility that they provide [1-3]. However, they are often simply used as a replacement for one or more conventional monolithic transducers with their set-up and operation designed to emulate an existing testing procedure. All current array controller systems are designed with this in mind and are typically set up to fire multiple elements with programmable time-delays between them so that the physical wavefront injected into the test-piece is equivalent to that from a monolithic transmitter. In this paper, this is referred to as parallel transmission. The received signals from elements in the array are recorded in parallel and then summed with appropriate time-delays to emulate the operation of an appropriate monolithic receiver. The concept of parallel transmission and reception originates in medical imaging where the

target is generally non-stationary and the overarching goal is to maintain an imaging frame rate that is as high as possible. To this end, medical imaging is a compromise between optimizing image quality and frame rate and many ingenious schemes have been designed [4-6] to achieve this that may use parallel transmission on a limited number of subsets of elements in conjunction with various coding schemes. Conversely, in the majority of NDE applications the target is time-invariant and the need for very high frame rates is not essential. Thus there is considerable scope in NDE applications for improving image quality and extracting more information from an array than in medical applications.

In order to maximize the flexibility of array signal processing, as much information as possible should be extracted from an array. The complete data set from an *n* element array has a finite size and is an *n*x*n* matrix of time-domain signals from every possible transmitter-receiver element combination. This is referred to as the full matrix and the procedure for obtaining it is referred to as full matrix capture (FMC). All possible processing algorithms, including all of those obtainable via conventional parallel transmission array operation may be implemented by post-processing the full matrix, together with an almost unlimited host of others.

2. Processing Methods

2.1. Total Focusing Method (TFM)

A key imaging algorithm that can only be performed practically by using post processing and FMC is the so-called total focusing method (TFM). The TFM yields a scalar image, $I(\mathbf{r})$, where the array is focused in transmission and reception at every point $\mathbf{r}$ in the image. Mathematically this can be written as:

$$I(\mathbf{r}) = \left| \sum_{i,j} g_{(i)j} \left(c\left|\mathbf{d}_{(\mathbf{i})}\right| + c\left|\mathbf{d}_{\mathbf{j}}\right| \right) \right| \tag{1}$$

where $g_{(i)j}(t)$ is the analytic time-domain signal when the i^{th} element transmits and the j^{th} element receives, c is the speed of sound in the test piece, and $\mathbf{d}$ is the vector between an element in the array and the point $\mathbf{r}$. This has been quantitatively shown by the authors [7] to provide superior resolution and image quality to any standard imaging approach. The TFM is sometimes referred to as the "gold standard" [8]. A number of experimental results obtained using the TFM and FMC on a variety of NDE specimens of different materials containing both real and artificial defects has already been published by the current authors [9].

As noted, the TFM produces the optimal image of reflector intensity. However it does not provide further information on the nature of reflectors. In particular small reflectors with wavelength order dimensions are too small for even the TFM to provide sufficient resolution in order to determine their shape. This is the motivation for probing the full matrix for more information on reflector characteristics.

2.2. Vector Total Focusing Method (VTFM)

The operation of the vector total focusing method (VTFM) can be described as follows with reference to Fig. 1:

- The array is subdivided into *N* equal sized sub-arrays (these may be overlapped) which act as different apertures. Let *j* denote the index of the sub-array.

- N TFM images, $I_j(\mathbf{r})$, are calculated over the complete grid of points in the image area using only data from array elements in the j^{th} sub-array.
- $I_j(\mathbf{r})$ is converted to a vector field, $\mathbf{V_j}(\mathbf{r})$, where the magnitude of vectors is equal to $I_j(\mathbf{r})$ and the orientation of vectors is towards the centre of the j^{th} sub-array aperture

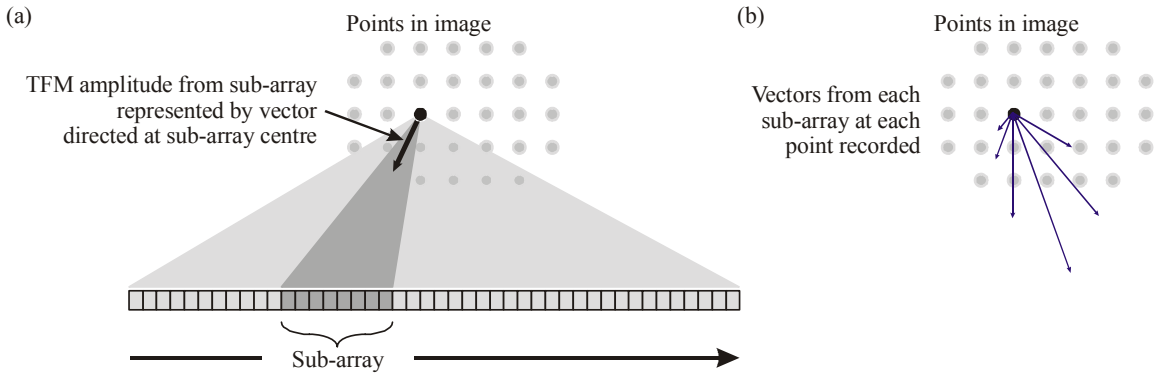

Fig. 1. Schematic diagrams indicating the operation of the basic VTFM algorithm showing (a) the vector generated from one sub-array aperture at a point in the image and (b) the vectors from a number of sub-array apertures at one point.

The result, $\mathbf{V_j}(\mathbf{r})$, is therefore an N-layered vector field. The computation of the VTFM vector fields is a subset of the overall TFM computation for the whole array. Therefore, other than increased data storage, the VTFM to this point does not require significant additional computational resource beyond that required to perform the TFM. The vector fields, $\mathbf{V_j}(\mathbf{r})$, are used firstly to determine the orientation of reflectors and secondly to determine how directional a reflector is by computing a quantity referred to as specularity.

To determine information about the orientation of the reflectors at a point in the image the following equation is used to process $\mathbf{V_j}(\mathbf{r})$:

$$\mathbf{V}(\mathbf{r}) = \left\{ \sum_{i=1}^{N} \{\mathbf{V}_i(\mathbf{r})\}^{\alpha} \right\}^{\frac{1}{\alpha}} \tag{2}$$

where the nomenclature $\{\mathbf{x}\}^y$ means that the magnitude of the vector $\mathbf{x}$ is raised to the y^{th} power but its direction is unchanged. If $\alpha = 1$ Eq. 2 represents a direct summation of the vector fields, $\mathbf{V_j}(\mathbf{r})$, and if $\alpha > 1$ then the sum is skewed towards the largest contributors. In the limit as α tends to infinity the result of Eq. 2 becomes simply equal to the vector in $\mathbf{V_j}(\mathbf{r})$ with the largest magnitude. A value of $\alpha = 4$ has been used to produce the results presented in the following section.

The specularity parameter, $S(\mathbf{r})$, is defined based on the standard deviation of vector lengths in $\mathbf{V_j}(\mathbf{r})$ at a point:

$$S(\mathbf{r}) = \frac{std\left(\left|\mathbf{V}_j(\mathbf{r})\right|\right)}{\sqrt{N}\ mn\left(\left|\mathbf{V}_j(\mathbf{r})\right|\right)} \tag{3}$$

where *std* and *mn* are the standard deviation and mean functions respectively and N is the number of apertures. It is straightforward to show that $0 \leq S(\mathbf{r}) \leq 1$ where $S(\mathbf{r}) = 0$ corresponds to point-like reflectors with uniform reflectivity in all directions and $S(\mathbf{r}) = 1$ corresponds to the extreme case of a reflector that has zero reflectivity to all but one sub-array position.

The reflector orientation, $\mathbf{V}(\mathbf{r})$, and specularity, $S(\mathbf{r})$, are both computed at all points in the image field. However, neither of these is ideal for use in isolation. The resolution of

$\mathbf{V}(\mathbf{r})$ is significantly lower than that $I(\mathbf{r})$ due to the aperture size of the sub-arrays necessarily being less then that of the whole array. Likewise, $S(\mathbf{r})$ has values at all locations regardless of whether or not a reflector is present, but the values away from reflectors are due to noise and are therefore meaningless. For this reason, both $\mathbf{V}(\mathbf{r})$ and $S(\mathbf{r})$ are currently used in conjunction with the TFM image, $I(\mathbf{r})$. For instance, the final vector field defining reflector orientation, $\mathbf{V}'(\mathbf{r})$, is defined as follows:

$$\mathbf{V}'(\mathbf{r}) = \frac{\mathbf{V}(\mathbf{r})}{|\mathbf{V}(\mathbf{r})|} I(\mathbf{r}). \tag{4}$$

This forces $|\mathbf{V}(\mathbf{r})|$ to equal $I(\mathbf{r})$, hence maintaining the optimum resolving power obtained from applying the TFM to the whole array while preserving the orientation of the vectors in $\mathbf{V}(\mathbf{r})$.

For illustrative purposes the specularity parameter is currently used to "tune" the TFM image to either point-like or specular reflectors. The tuned image, $I'(\mathbf{r})$, is given by:

$$I'(\mathbf{r}) = [S(\mathbf{r})]^{\beta} I(\mathbf{r}) \tag{5}$$

where β is the tuning parameter. If $\beta = 0$ the image is the unmodified TFM image. If $\beta > 0$ specular reflectors are emphasized and if $\beta < 0$ point-like reflectors are emphasized.

2.3. Time of Flight Diffraction (TOFD) and Diffraction Total Focusing Method (DTFM)

The time of flight diffraction (TOFD) inspection method was first introduced in the 1970s and employs two probes in a pitch-catch arrangement and is often used for the sizing of defects in welds. Interpretation of TOFD data requires considerable skill. Here it is suggested that the use of twin arrays rather than monolithic probes has the potential to significantly improve the performance of the TOFD configuration and make the resulting data more easily interpretable. The principle is to apply the TFM algorithm to the data from the two arrays to create an image in the cross-sectional plane through the test-piece at each position as the arrays are scanned along a sample. The physics of defect detection remains the same as in TOFD in that DTFM is based on the diffraction of ultrasound at the tips of crack-like defects. There are a number of possibilities for producing DTFM images: (a) apply the TFM to data from all elements in both arrays, effectively creating a longer array with a gap in the centre, (b) apply the TFM to the data from each array independently and (c) apply the TFM to simulate transmission on one array and reception on the second. Here the results for (a) and (c) are presented.

3. Experimental Procedure

3.1. Samples

Tests were performed on the two samples shown in Fig. 2. The first was an aluminium block containing one Ø1 mm hole and five 1 mm by 0.3 mm slots at various angles cut into the block using wire electrical discharge machining (EDM). The second was a stainless steel plate sample with areas of two different thicknesses separated by a tapered section. The tapered section contained a number of artificial defects of the type found in welds.

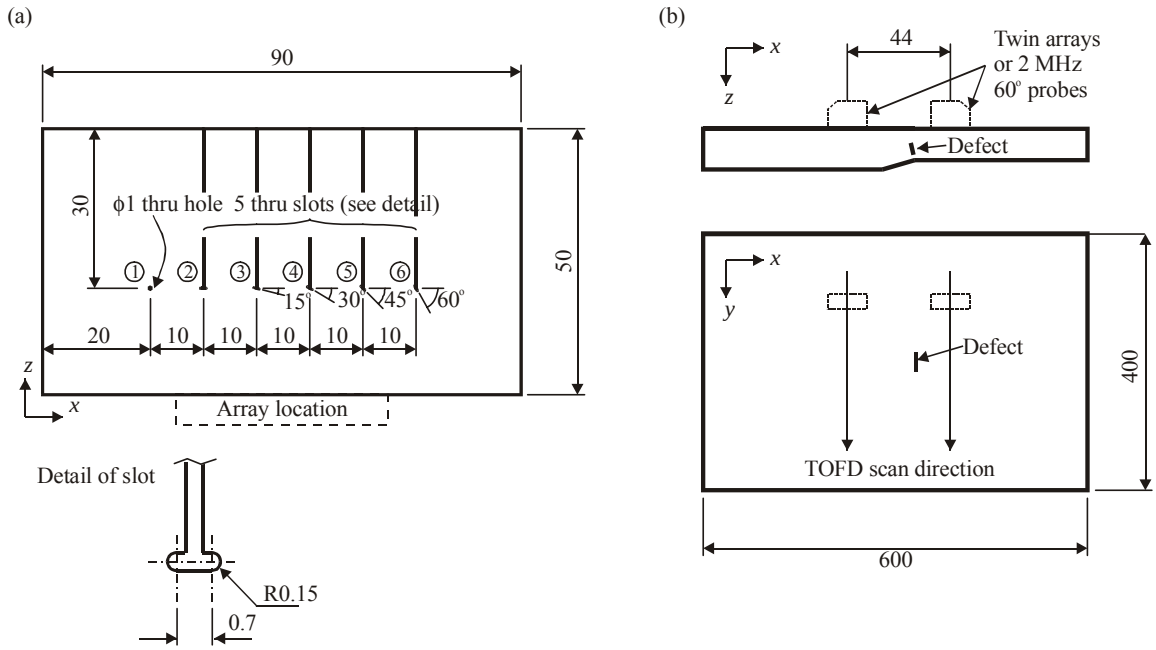

Fig. 2. Samples used: (a) aluminium block containing wire EDM slots at various angles; (b) stainless steel specimen containing simulated weld defects.

3.2. Array Testing

A commercial array controller (Micropulse MP5PA manufactured by Peak NDT Ltd., Derby, UK) that contains 64 parallel transmission and reception channels was used to perform full matrix capture (FMC). For all tests the acquired data was post-processed using Matlab (The Mathworks Inc., Natick, MA). The first stage of processing was to convert the real time-domain signals, $f_{(i)j}(t)$, to analytic signals, $g_{(i)j}(t)$, using a Hilbert transform. At the same time, a digital frequency domain filter, $D(\omega)$, was applied to eliminate out-of-bandwidth noise:

$$g_{(i)j}(t) = \frac{1}{\pi}\int_0^\infty F_{(i)j}(\omega)D(\omega)e^{-i\omega t}d\omega \text{ where } F_{(i)j}(\omega) = \int_{-\infty}^{\infty} f_{(i)j}(\omega)e^{i\omega t}dt\,. \qquad (6)$$

The filter used was a Gaussian band-pass filter with a -40 dB pass-band from 2.5 to 7.5 MHz. Linear arrays with 5 MHz centre frequency manufactured by Imasonic (Besançon, France) were used for all the experimental work described. The element dimensions in all arrays were 15 x 0.53 mm and the spacing between elements was 0.1 mm, resulting in an element pitch of 0.63 mm. The array used on the aluminium sample comprised 64 elements and was used to obtain data for the TFM and VTFM processing. This array was used at a fixed position as shown in Fig. 2(a). The second 'array' used to obtain data for DTFM processing on the stainless steel sample was actually a pair of 32 element arrays wired to a common connector. This pair of arrays were scanned along the sample as indicated in Fig. 2(b), although here only the results obtained at a single scan position at a defect location are presented.

3.3. Time of Flight Diffraction (TOFD) Testing

Conventional time of light diffraction (TOFD) scans were carried out on the stainless steel sample as indicated in Fig. 2(b). For this purpose, a pair of 2 MHz transducers on 60º wedges that were connected in pitch catch mode to a standard pulser-receiver. A digital

storage oscilloscope was used to record the signals which were then imported into Matlab for processing.

4. Experimental Results

4.1. Total Focusing Method (TFM)

The results from the TFM algorithm applied to data obtained from the 64 element array on the aluminium sample are shown in Fig. 3. From the image it can be seen that all six reflectors are clearly visible but that the shape and type of reflector cannot be deduced from the image. The shape of the individual signal from each reflector is entirely due to the position of the reflector relative to the array and is approximately equal to the point spread function (PSF) of the array at that point.

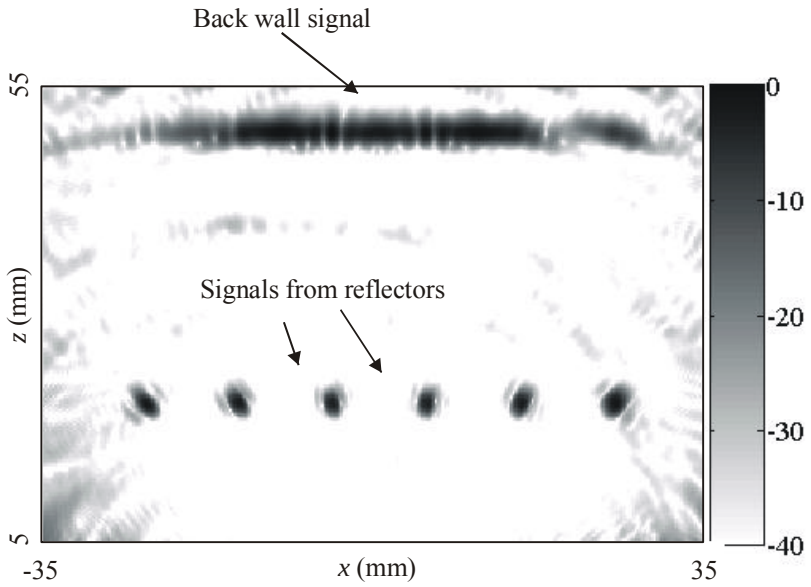

Fig. 3. TFM image obtained from aluminium sample. The greyscale is in dB relative to the largest reflector which is the back wall of the sample.

4.2. Vector Total Focusing Method (VTFM)

The results from processing the data from the aluminium sample using the VTFM algorithm to compute reflector orientation are shown in Fig. 4. It can be seen that for the five slot reflectors, the orientation of the vectors in the vector image clearly points in the direction normal to the angle of the slot. For the circular hole the vectors appear to indicate a reflector facing the centre of the array.

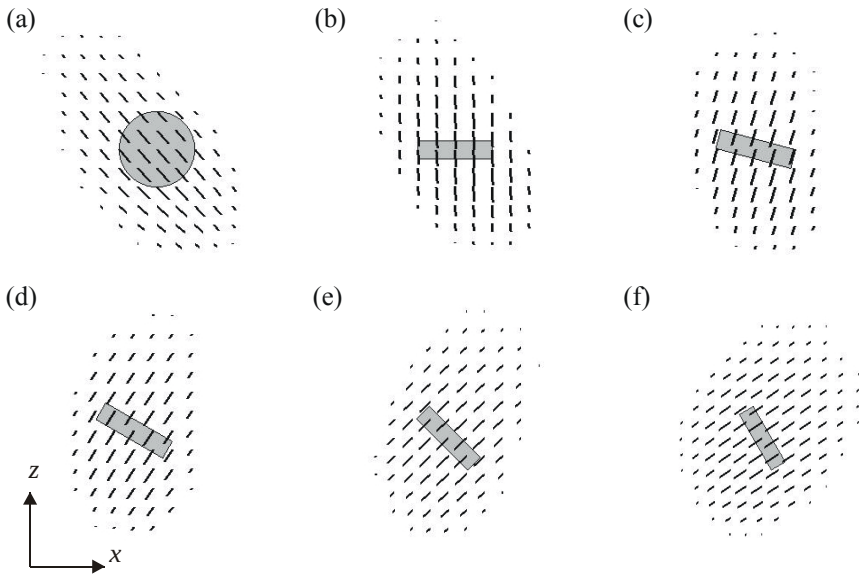

Fig. 4. Detail of VTFM vector field images of reflector orientation from the six reflectors in the aluminium sample: (a) Ø1 mm hole; (b) slot at 0º; (c) slot at 15º; (d) slot at 30º; (e) slot at 45º; (f) slot at 60º.

Fig. 5 shows the TFM image in Fig. 3 tuned using the specularity measurement according to (5). In this figure it can be seen that the specularity parameter allows discrimination between the non-specular (i.e. Ø1 mm circular hole) and specular reflectors (i.e. the 1 mm by 0.25 mm slots).

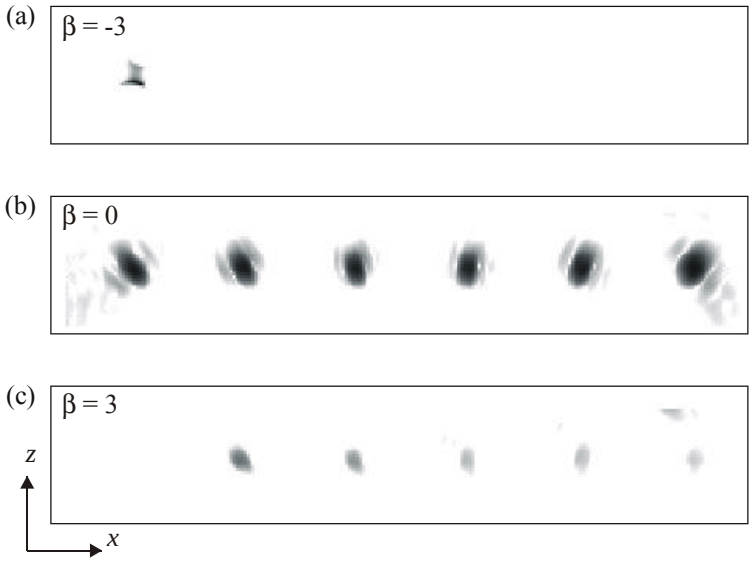

Fig. 5. TFM images tuned using specularity parameter: (a) tuned to highlight non-specular reflectors; (b) untuned; (c) tuned to highlight specular reflectors.

4.3. Diffraction Total Focusing Method (DTFM)

A section of the TOFD image obtained from the pair of monolithic transducers is shown in Fig. 6(a). In this image, the transducers are being scanned past one of the defects in the plate, the signal from which is indicated in the figure. The defect signal is clear and a skilled operator could estimate its lateral extent in the (*y* direction) from this image. In order to determine its depth and other dimensions, a further scan would be required in the *x* direction.

The twin arrays were scanned along the sample in the *y* direction and the DTFM processing applied to the full data set at each scan point. Here the resulting DTFM images at a position near the centre of the defect shown in Fig. 6(a) are shown in Figs. 6(b) and (c). The difference between the images is that in Fig. 6(b) the TFM algorithm is applied to the data from all elements in both arrays and in Fig. 6(c) the TFM algorithm is applied so that one array acts as a transmitter and the second as a receiver. The advantage of using arrays is that an instantaneous cross sectional image in the *x*-*z* plane is obtained at each scan position in the *y*-direction, hence enabling defects to be sized directly from the images. This is in contrast to conventional TOFD inspection where sizing in the *x*-*z* plane requires further scanning and advanced interpretation of the resulting data. A further advantage of DTFM is that the signal to noise ratio is higher than TOFD since the transmitter and receiver are focussed at each point in turn, whereas in TOFD divergent beams are used.

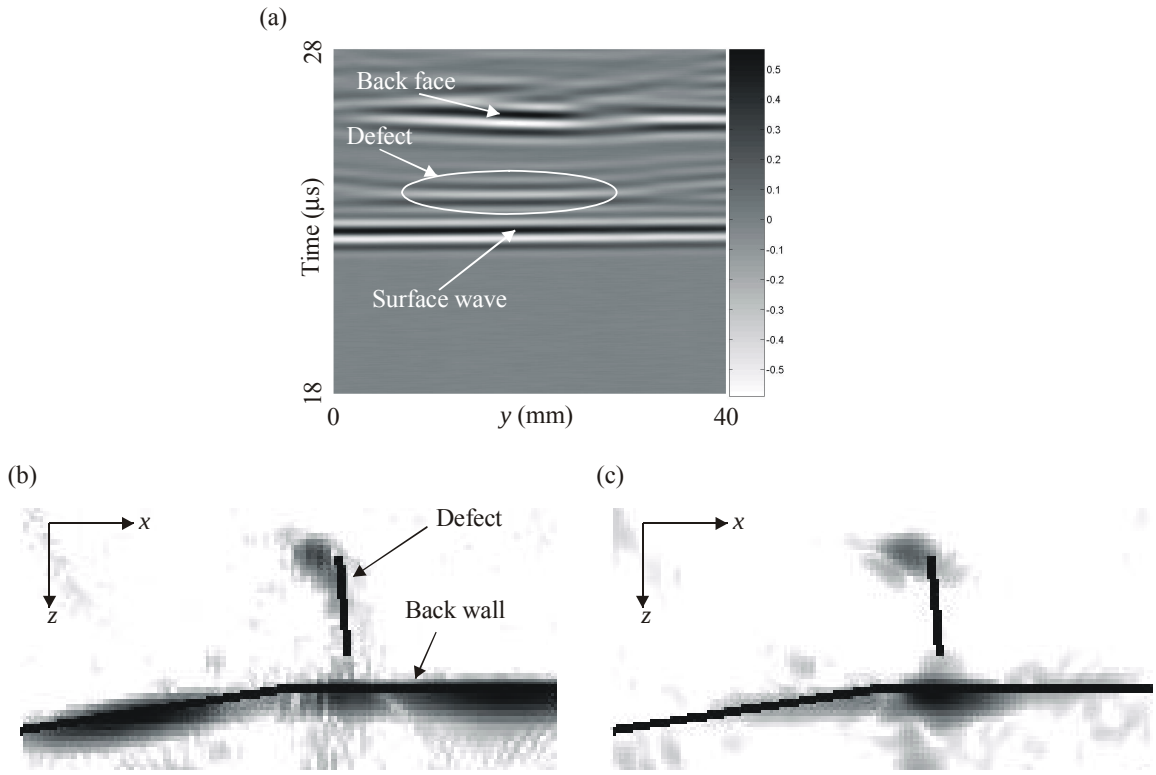

Fig. 6. (a) TOFD image from defect in stainless steel sample and DTFM images from the same defect: (b) using all elements in both arrays; (c) using the elements in one array to transmit and elements in the second array to receive.

5. Conclusion

Several signal processing strategies that exploit the full matrix of time-domain data from an ultrasonic array have been discussed and demonstrated experimentally. It has been shown that advanced processing can be used to characterise sub-wavelength defects in terms of their orientation and specularity. It has further been suggested that the use of twin arrays is a superior method of defect sizing to the conventional TOFD technique.

Acknowledgement

This work was supported through the core research programme within the UK Research Centre in NDE (RCNDE) funded through EPRSC grant number: GR/S09388/01.

References

[1] S. J. Song, H. J. Shin and Y. H. Jang, *Nucl. Eng. & Des.*, 214, 151-161 (2002).
[2] R. A. Smith, J. M. Bending, L. D. Jones, T. R. C. Jarman and D. I. A. Lines, *Insight*, **45**(3), 174-177 (2003).
[3] S. Mahaut, O. Roy, C. Beroni and B. Rotter, *Ultrasonics*, **40**, 165-169 (2002).
[4] R. Y. Chiao and X. H. Hao, *IEEE Trans. Ultrason., Ferroelec. & Freq. Contr.*, **52**(2), 160-170 (2005).
[5] T. H. Gan, D. A. Hutchins, R. J. Green, M. K. Andrews and P. D. Harris, *IEEE Trans. Ultrason., Ferroelec. & Freq. Contr.*, **52**(2), 280-288 (2005).
[6] T. Misaridis and J. A. Jensen, *IEEE Trans. Ultrason., Ferroelec. & Freq. Contr.*, **52**(2), 177-219 (2005).
[7] C. Holmes, B. W. Drinkwater and P. D. Wilcox, "Post-processing of the Full Matrix of Ultrasonic Transmit-receive Array Data for Non-destructive Evaluation", *NDT and E Int.*, **38**(8), pp 701-711 (2005).
[8] O. Oralkan, A. Sanh Ergun, J. A. Johnson, M. Karaman, U. Demirci, K. Kaviani,T. H. Lee, B. T. Khuri-Yakub, *IEEE Trans. Ultrason., Ferroelec. & Freq. Contr.*, **49**, 1596-1610 (2002).
[9] C. Holmes, B. W. Drinkwater and P. D. Wilcox, *Insight*, **46**(11), 677-680 (2005).